Molecular Therapy
Original Article

Cell-penetrating peptide-conjugated Morpholino rescues SMA in a symptomatic preclinical model

Margherita Bersani,[1,6] Mafalda Rizzuti,[2,6] Elisa Pagliari,[1] Manuela Garbellini,[3] Domenica Saccomanno,[2] Hong M. Moulton,[4] Nereo Bresolin,[1,2] Giacomo P. Comi,[1,2,5] Stefania Corti,[1,2,7] and Monica Nizzardo[2,7]

[1]Dino Ferrari Centre, Neuroscience Section, Department of Pathophysiology and Transplantation (DEPT), University of Milan, Milan, Italy; [2]Foundation IRCCS Ca' Granda Ospedale Maggiore Policlinico, Neurology Unit, Milan, Italy; [3]Healthcare Professionals Department - Foundation IRCCS Ca' Granda Ospedale Maggiore Policlinico, Milan, Italy; [4]Department of Biomedical Sciences, Carlson College of Veterinary Medicine, Oregon State University, Corvallis, OR, USA; [5]Foundation IRCCS Ca' Granda Ospedale Maggiore Policlinico, Neuromuscular and Rare Diseases Unit, Milan, Italy

Spinal muscular atrophy (SMA) is a motor neuron disease and the leading genetic cause of infant mortality. Recently approved SMA therapies have transformed a deadly disease into a survivable one, but these compounds show a wide spectrum of clinical response and effective rescue only in the early stages of the disease. Therefore, safe, symptomatic-suitable, non-invasive treatments with high clinical impact across different phenotypes are urgently needed. We conjugated antisense oligonucleotides with Morpholino (MO) chemistry, which increase SMN protein levels, to cell-penetrating peptides (CPPs) for better cellular distribution. Systemically administered MOs linked to r6 and $(RXRRBR)_2XB$ peptides crossed the blood-brain barrier and increased SMN protein levels remarkably, causing striking improvement of survival, neuromuscular function, and neuropathology, even in symptomatic SMA animals. Our study demonstrates that MO-CPP conjugates can significantly expand the therapeutic window through minimally invasive systemic administration, opening the path for clinical applications of this strategy.

INTRODUCTION

Spinal muscular atrophy (SMA) is an autosomal-recessive, degenerative motor neuron disease, and is the main genetic cause of infant mortality.[1] SMA patients show progressive loss of motor neurons (MNs) in the ventral horns of the spinal cord, causing progressive muscle weakness, paralysis, and premature death. Homozygous mutations of the survival motor neuron 1 gene (*SMN*) account for reduced levels of SMN protein, which is critically important for MN maintenance and survival.[1,2] Humans have a nearly identical copy of the *SMN* gene, *SMN2*, which differs from *SMN* in five nucleotides. One of them determines the exclusion of exon 7 in *SMN2*, producing a truncated, non-functional SMN protein in 90% of cases.[3] *SMN2* copy number varies among individuals and is the most important influence on the clinical phenotype.[4]

Currently, three disease-modifying treatments are approved by the US Food and Drug Administration: nusinersen, onasemnogene abeparvovec, and risdiplam. Nusinersen is an antisense oligonucleotide (ASO) that modulates *SMN2* splicing by promoting the inclusion of exon 7 and the production of a functional SMN protein. It requires repeated intrathecal administration,[5,6] a relatively invasive procedure with side effects related to lumbar puncture, such as headache, local pain, etc. In addition, late-onset patients are often affected by scoliosis, have undergone previous spine fusion operations, and frequently have joint contractures and respiratory insufficiency, which complicate lumbar puncture.[7] Indeed, with currently available ASOs, limited distribution of the molecules to the rostral spinal and brain regions in some patients likely hamper the clinical response of their motor units in these regions.[8] Moreover, recent reviews have provided evidence that nusinersen can improve with heterogeneity motor functions in SMA type I and II but not always in SMA type III subjects.[9] Onasemnogene abeparvovec is a gene therapy that provides wild-type full-length SMN cDNA. It is systemically delivered, but its long-term persistence in peripheral organs is not yet determined and it has been linked to serious immunological side effects, particularly in the liver.[10] As yet, no clinical data are available regarding its use in SMA II–IV. Risdiplam is a small molecule that increases SMN production from *SMN2* mRNA. It has the great advantage of being orally administered and systemically distributed, but possible nonspecific effects of the molecule can lead to unexpected adverse side reactions. All SMN-based approved therapies show a very narrow therapeutic window: the compounds are strikingly efficient only in the pre- or early symptomatic phases, for reasons not completely understood,[11] and delayed intervention leads to a less efficient rescue of the pathological phenotype.[12] As SMA patients are a very heterogeneous group, the only identified factor that is predictive of SMN-augmenting treatment success is the age of the patient at treatment initiation, which is closely related to disease duration.[11] Nevertheless, universal newborn screening remains a very distant prospect. Thus, we sorely lack a drug

Received 5 November 2020; accepted 16 November 2021;
https://doi.org/10.1016/j.ymthe.2021.11.012.

[6]These authors contributed equally

[7]These authors contributed equally

Correspondence: M. Nizzardo, Neuroscience Section, Department of Pathophysiology and Transplantation (DEPT), University of Milan, Neurology Unit, IRCCS Foundation Ca' Granda Ospedale Maggiore Policlinico, Via Francesco Sforza 35, 20122 Milan, Italy.
E-mail: monica.nizzardo1@gmail.com

suitable for treating symptomatic SMA patients across different clinical phenotypes.

Overall, since ASOs are sequence specific and their administration can be stopped, thus increasing their safety, they are the most promising therapies to be further optimized.[10] Data collected on autoptic material demonstrated a 6.5-fold decline in normal SMN protein expression in the human non-SMA spinal cord between the fetal and post-natal stages, up to the third month of post-natal life.[13] Moreover, data on the efficacy of splicing modulation in SMA types II and III showed interesting effects on phenotype that might depend on SMN's effects well beyond immediate post-natal life.[8] Therefore, treatment SMA in the symptomatic phase could be beneficial and should be investigated.

Here, we aimed to address these issues by developing novel ASO compounds that do not require invasive injection, have local and systemic actions, and are remarkably effective in symptomatic SMA. In previous experiments, we and other groups have already demonstrated the efficacy of a specific ASO sequence, synthesized with Morpholino (MO) chemistry, in targeting the ISS-N1 region within *SMN2* (HSMN2Ex7D 10–34), leading to robust improvement of pathologic hallmarks with pre-symptomatic administration in SMA pups.[14,15]

In this study, we investigated whether the biodistribution and overall efficacy of our MO treatment could be increased by conjugation with cell-penetrating peptides (CPPs), small cationic arginine-rich peptides that have already shown great potential as transmembrane delivery agents for macromolecular compounds.[16,17] The efficacy of CPPs in enhancing the systemic delivery of MOs has already been demonstrated in a Duchenne muscular dystrophy (DMD) mice model[18,19] and in pre-symptomatic SMA transgenic rodents,[20,21] but it has never been assessed in symptomatic SMA stages. After pilot experiments to select the best CPP-MO conjugates, we explored the potential of r6- and $(RXRRBR)_2XB$ (RXR)-MO to improve the disease phenotype in symptomatic SMA mice after systemic delivery. We demonstrated the superiority of the CPP-MO conjugates in comparison with the naked MO in increasing SMN protein levels, improving the pathological phenotype, extending the lifespan of the mice, and rescuing histopathological features through a single systemic injection, without any detectable toxic effects. Based on our results, CPP-MO conjugates can be considered a very promising, novel, safe, non-invasive, and efficient therapy suitable to be translated to the clinic for symptomatic patients and those with milder SMA unable to take advantage of available treatments.

RESULTS

CPP-conjugated MOs are able to increase SMN protein levels in the CNS

We conjugated our validated MO sequence targeting the ISS-N1 region within *SMN2* (HSMN2Ex7D 10–34)[15] with one of four different CPPs (Tat, R6, r6, and RXR). To verify the ability of each CPP to deliver the MO to the CNS and increase the amount of SMN protein, and to select the most efficient conjugate for further experiments, we performed an intracerebroventricular (ICV) (Figures S1A, S1C, and S1E) or intravenous (IV) (Figures S1B, S1D, and S1F) injection with the four different CPP-MOs at a concentration of 12 nmol/g body weight in heterozygous SMAΔ7 mice at post-natal day 1 (P1). Western blot (WB) results confirmed the superiority of CPP-conjugated MOs in significantly increasing the level of SMN protein in both brain (Figures S1C and S1D) and spinal cord (Figures S1C–S1F, $p < 0.001$ in brain ICV; $p < 0.05$ in brain IV and spinal cord ICV; $p < 0.01$ in spinal cord IV). The r6 and RXR peptides were the most effective in rescuing SMN if compared with naked MO ($p < 0.05$). Therefore, these peptides were selected for the subsequent experiments in symptomatic SMA mice.

CPPs deliver MOs to the CNS and peripheral organs of symptomatic SMAΔ7 mice

We tested the selected RXR-MO and r6-MO conjugates in SMAΔ7 mice at P5, which corresponds to a symptomatic phase of SMA. We injected the scrambled control (scr-MO), the naked MO, and the r6/RXR-conjugated MO at the concentration of 12 nmol/g by systemic intraperitoneal (IP) injection. Mice (n = 4/group) were sacrificed 48 h after treatment. WB analysis of brain and spinal cord revealed a striking increase in SMN protein in mice treated with the CPP-MO conjugates (Figure 1A). Statistically significant results were obtained in the brains ($p < 0.05$, Figure 1B) and in the spinal cord ($p < 0.01$, Figure 1C) of mice treated with conjugates. These data demonstrated that systemically administered select CPPs can deliver MO to the CNS, even in a symptomatic phase, when the blood-brain barrier (BBB) is completely closed. Further WB analyses were performed on heart, liver, and kidney (Figure 1D), and confirmed the significant increase in SMN levels in the livers and hearts ($p < 0.01$, Figure 1E), as well as in the kidneys ($p < 0.05$, Figure 1E) of CPP-treated mice. We also tested lower doses of conjugates by injecting IP 6 and 9 nmol/g (n = 3/group), but WB analysis showed no difference in SMN levels in the CNS after those treatments (data not shown).

To collect data about the real biodistribution of naked MO and CPP-MOs, independent from the SMN level, we performed an enzyme-linked immunosorbent assay (ELISA) assay designed to specifically detect our MO sequence. We assessed MO levels in brain, spinal cord, heart, quadriceps, and liver of symptomatic SMA mice treated at P5 with naked MO and r6-MO, which is the best peptide according to WB, by IP injection (Figure 1F). Conjugation with r6 allowed MO to reach all of these organs, with an average MO detection of 7,298 pM in spinal cord, 5,271 pM in heart, 85,780 pM in liver, and 6,061 pM in muscle. Our data showed a significantly higher amount of MO delivered by the r6 peptide compared with the naked MO in liver ($p < 0.05$), spinal cord ($p < 0.05$), muscle ($p < 0.05$), and heart ($p < 0.001$). In brain samples, we found only a trend toward increase (data not shown), but basal values were always low and not reliable, suggesting possible technical problems related to this specific tissue.

CPP-MOs treatment in a symptomatic phase rescues the phenotype in SMAΔ7 mice

To evaluate the effects of CPP-conjugated MOs on the disease phenotype, we treated symptomatic SMAΔ7 mice at P5 with 12 nmol/g of

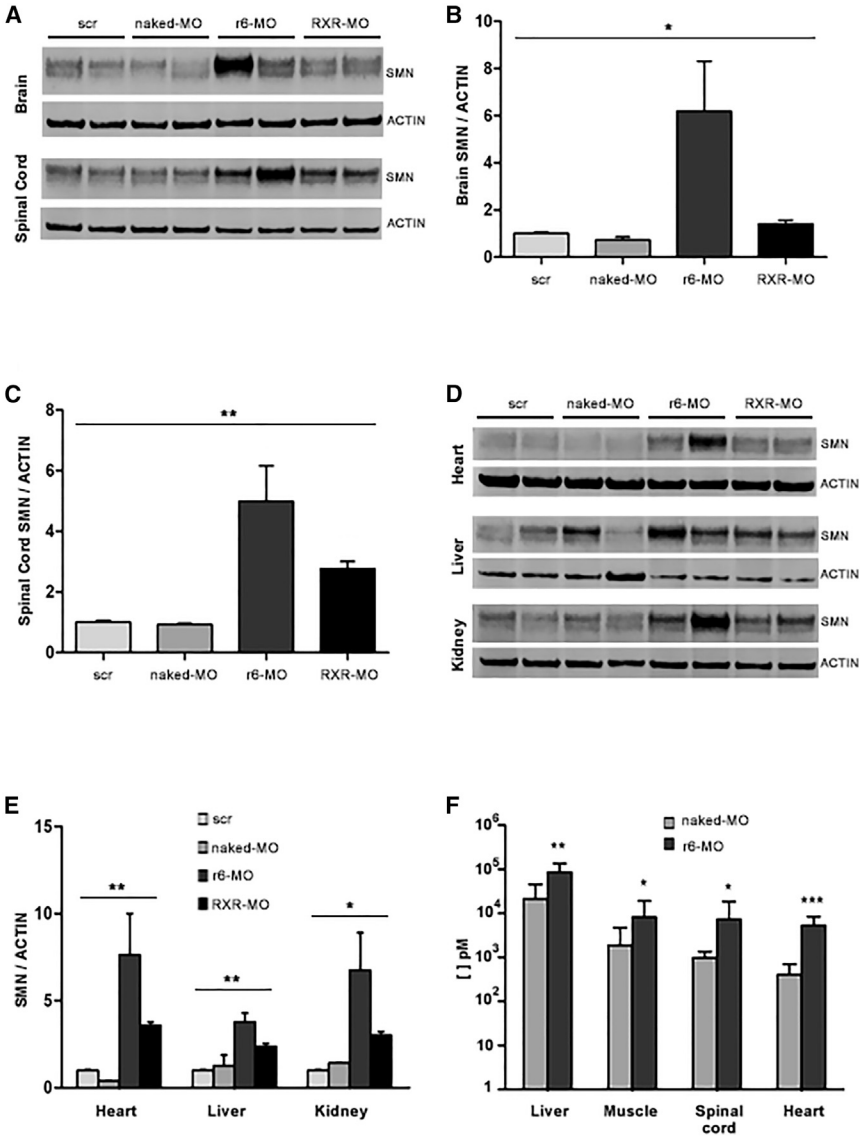

Figure 1. Treatment with CPP-MOs by IP injection at P5 increases SMN levels and delivers MOs to multiple organs in SMA mice

Representative image of WBs for SMN and actin (A and D) and their densitometric analysis (B, C, and E) performed on protein extracted from brain (B), spinal cord (C), and heart, liver, and kidney (E) from SMA mice treated IP at P5 with 12 nmol/g of naked MO, r6-MO, or RXR-MO, and sacrificed at P7. Scr-MO animals were used as controls (four mice/group). Relative amounts of SMN were normalized to actin levels as mean ± SEM. Statistical significance was determined using one-way ANOVA (*$p < 0.05$, **$p < 0.01$) and Student's t test comparing CPP-MOs versus naked MO ($p < 0.05$). (F) Stacked bar plot of ELISA assay results for MO presence in brain, spinal cord, liver, heart, and muscle from SMA mice treated IP at P5 with 12 nmol/g of naked MO or r6-MO, and sacrificed at P7. Scr-MO animals were used as controls. Statistical significance was determined using Student's t test comparing CPP-MO versus naked MO (*$p < 0.05$, **$p < 0.01$, ***$p < 0.001$, at least three mice/group).

r6-MO or RXR-MO (n = 8/group), compared with naked MO mice (n = 10). Mice injected with the scr-MO (n = 12) were used as controls. Treated mice were monitored daily with regard to the phenotypic disease hallmarks and survival, until the end stage. Mice treated with the scr or naked MO presented cases of paralysis and death in the first 2 weeks, with a median lifespan of 12 days for the scr-MO and 17 days for the naked MO symptomatic mice (Figure 2A). Scr-MO and naked MO mice presented muscle weakness starting from the injection day (P5). Indeed, when laid on their backs, they were not able to turn and stand on four paws in the righting test (Figure 2B; Video S1) and, when suspended by the tail, they were not able to extend their hind limbs during the tube test (Figure 2C) and never reached the age (45 days) to perform the rotarod test. Treatment with either CPP-conjugated MO significantly improved the survival and functional condition of symptomatic SMA mice compared with scr-MO and naked MO mice. Kaplan-Meier curves showed an overall statistically significant increase in survival with CPP-MOs ($p < 0.001$, $\chi^2 = 45.39$, Figure 2A). Strikingly, when compared with the naked MO, CPP-MOs improved median survival (17 days for the naked MO) to 41.4 days for r6-MO ($p < 0.001$, $\chi^2 = 16.91$) and 23 days for RXR-MO ($p < 0.01$, $\chi^2 = 9.157$, Figure 2A). CPP-MO-treated mice did not develop eye or ear necrosis after month 5, maintained good motor skills and autonomous movement (Video S2), and presented better performance compared with naked MO mice in the righting test at different time points (for r6-MO $p < 0.001$, all time points; for RXR-MO $p < 0.001$ at P10 and $p < 0.05$ at P13, Figure 2B; Video S3). The improvement related to the naked MO was also observed in the tube test at P10 ($p < 0.05$ for r6-MO) and at P13 ($p < 0.001$ for r6-MO, $p < 0.05$ for RXR-MO, Figure 2C), and in the results of the rotarod test (Figure 2D; Video S4), which was successfully completed by the majority of CPP-MO mice. Comparing the two CPP-MOs, r6-MO-treated mice always performed better than RXR-MO mice, showing greater efficacy in rescuing the disease phenotype.

To further investigate the therapeutic window of CPP-MO treatment, we also treated SMA mice at P7 and P10 by IP injection. We observed that survival did not improve compared with naked MO- and scr-MO-treated mice (average survival: 13.1 days for r6-MO and 15.2 days for RXR-MO, data not shown). Moreover, we treated SMA mice at P7 by ICV injection to be sure the entire dose of

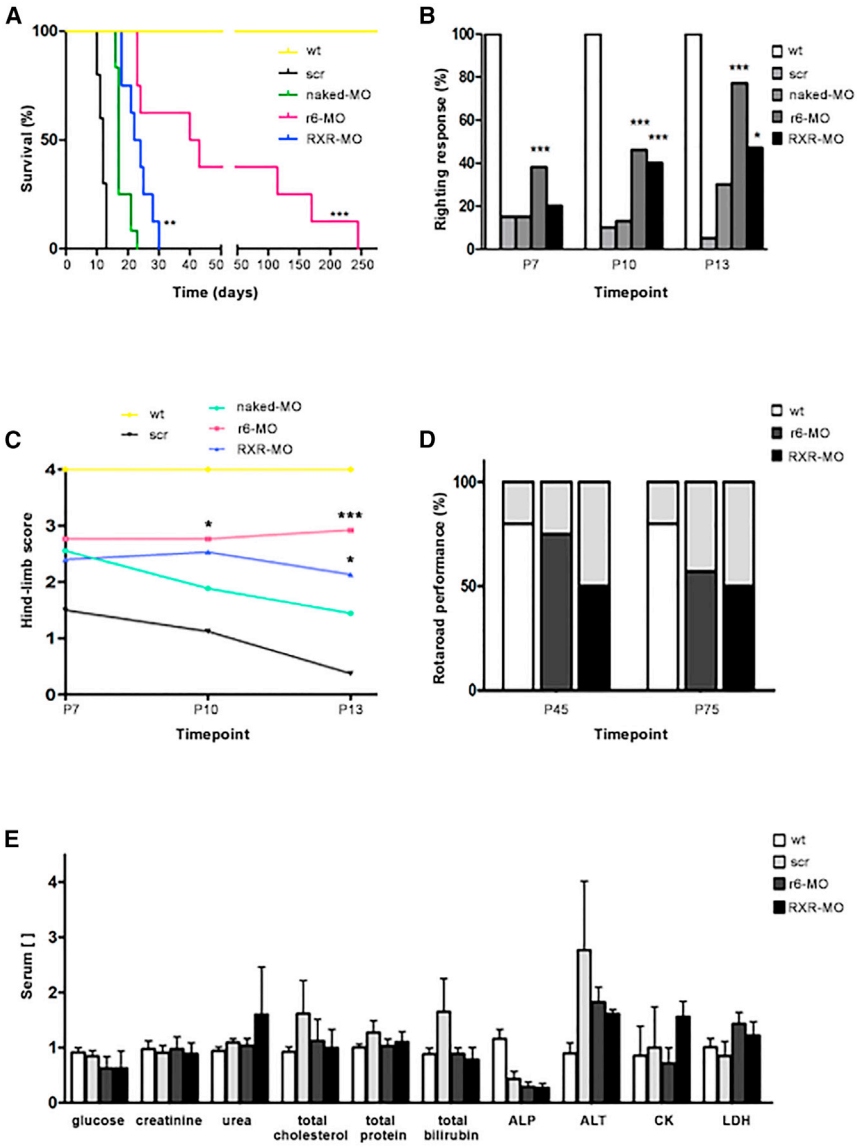

Figure 2. Treatment with CPP-MOs by IP injection at P5 extends the survival and ameliorates the phenotype of SMA mice

(A) Kaplan-Meier survival curve of wild-type and SMA mice treated IP at P5 with scr-MO (n = 10), naked MO (n = 12), r6-MO, or RXR-MO (n = 8/group); CPP-MOs significantly enhanced survival (***p < 0.001, $\chi 2$ = 14.59, **p < 0.01, $\chi 2$ = 9.157). (B) Stacked bar plot of the percentage of positive righting reflex responses in wild-type and SMA mice treated IP at P5 with naked MO, r6-MO, or RXR-MO at three different time points showing improvement with CCP-MO in comparison with naked MO treatment (scr-MO n = 10, naked MO n = 12, r6-MO, RXR-MO n = 8, r6-MO: ***p < 0.001, all time points; RXR-MO: ***p < 0.001 at P10 and *p < 0.05 at P13, contingency and Fisher's exact tests, CPP-MO versus naked MO). (C) Mean tube test hindlimb scores on a 0–4 scale. SMA mice were treated IP at P5 with scr-MO, naked MO, r6-MO, or RXR-MO at three different time points. Mice treated with CPP-MOs performed significantly better than mice treated with naked MO (scr-MO n = 10, naked MO n = 12, r6-MO, RXR-MO n = 8, r6-MO: *p < 0.05 at P10 and ***p < 0.001 at P13, RXR-MO: *p < 0.05 at P13, Student's t test, CPP-MO versus naked MO). Values are presented as means ± SEM. (D) Stacked bar plot of rotarod performance test results of wild-type and SMA mice treated IP at P5 with r6-MO or RXR-MO. No scr-MO or naked MO mice were alive at the two time points tested. Results are indicated as the percentage of animals that completed the test (p < 0.001 r6-MO versus RXR-MO at P45). The records were performed at two different time points P45 and P75. (E) Stacked bar plot of toxicity markers analyzed in wild-type (n = 11) and SMA mice treated at P5 with 12 nmol/g of r6-MO and RXR-MO (n = 3/group, one-way ANOVA. p < 0.05 for ALP and ALT). Measurement units for concentrations: mg/dL for glucose, creatinine, urea, total cholesterol, total bilirubin; g/dL for total protein; U/L for alkaline phosphatase (ALP), alanine transaminase (ALT), creatine kinase (CK), and lactate dehydrogenase (LDH).

treatment could reach the brain, but observed no remarkable increase in lifespan, suggesting that treatment at P7 is too late to obtain any rescue of the disease (data not shown).

To evaluate possible toxic effects caused by CPP-MO treatment, we collected serum from wild-type mice and symptomatic mice IP treated with scr-MO, r6-MO, or RXR-MO. Toxicological evaluation was performed on a standard set of biomarkers for liver and kidney toxicity, such as glucose, creatinine, urea, total cholesterol, total protein, total bilirubin, alkaline phosphatase, alanine transaminase, creatine kinase, and lactate dehydrogenase. All biomarker levels were comparable between the groups, suggesting that the treatments had no detectable toxic effects (Figure 2E).

CPP-MO treatment ameliorates pathological hallmarks in spinal cord and muscles of SMA mice

SMAΔ7 mice develop neuropathological features starting from P5. One of them is the degeneration of neuromuscular junctions (NMJs), whose denervation increases with the progression of the disease.[22] The disease is also characterized by marked and progressive MN degeneration.[23] To better understand the mechanisms underlying phenotypic rescue after CPP-MO treatment, we analyzed scr-MO, naked MO, r6-MO, and RXR-MO mice treated by IP injection at P5 and sacrificed at P10 or P30 (n = 4/group). The pathological hallmarks were observed in all the untreated, scr-MO, and naked MO mice at P10. Analyses at P30 could not be performed in these animals since they died around P15. Interestingly, in CPP-treated mice, we observed a marked amelioration

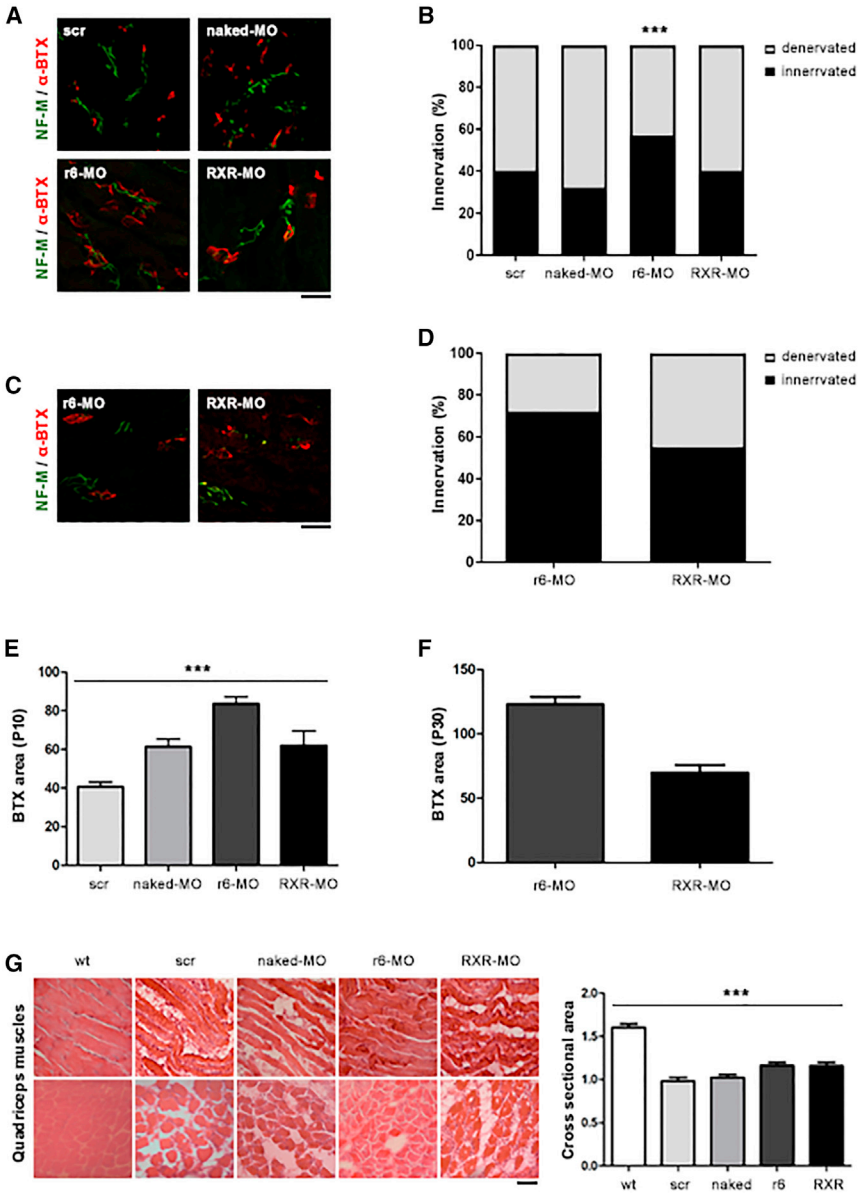

Figure 3. Treatment with CPP-MOs ameliorates intercostal muscle NMJ innervation in SMA mice

(A) Immunostaining of intercostal muscles from symptomatic SMA mice treated at P5 with scr-MO, naked MO, r6-MO, or RXR-MO sacrificed at P10, performed with NF-M antibody (green) and α-bungarotoxin antibody (red). Magnification: 40×. (B) Stacked bar plot of the percentage of innervated (black) and denervated (light gray) NMJs in SMA mice at P10 (**p < 0.01, for r6-MO, n = 100 NMJs, 4 mice/group, contingency and Fisher's exact test, CPP-MO versus naked MO). (C) Representative image of NMJ staining of SMA mice treated with r6-MO or RXR-MO and sacrificed at P30. (D) Stacked bar plot of the percentage of innervated (black) and denervated (light gray) NMJs in SMA mice at P30 (n = 100 NMJs, 4 mice/group). (E and F) Stacked bar plot of endplate area of NMJs in SMA mice at P10 (E) and P30 (F) (***p < 0.001, n = 100 BTXs, n = 4 mice/group, one-way ANOVA). (G) Representative image of hematoxylin and eosin staining of quadriceps muscles from SMA mice treated with scr-MO, naked MO, r6-MO, or RXR-MO and wild-type mice, sacrificed at P10 (magnification: 40×) and stacked bar plot of cross-sectional area of muscle fibers in SMA mice at P10 (***p < 0.001, n = 100 fibers, n = 4 mice/group, one-way ANOVA). Scale bars, 75 μm (A and C) and 90 μm (G).

of NMJ denervation at P10 compared with naked MO, 5 days after treatment, which was significant for r6-MO ($p < 0.001$, Figures 3A and 3B). The recovery of peripheral synapses in r6-MO mice reached 60% innervation, while it did not surpass 40% in scr-MO and naked MO mice (Figure 3B). At P30, innervation remained good, at 72% in r6-MO and 50% in RXR-MO-treated mice, again confirming the superiority of r6-MO treatment ($p < 0.05$ r6-MO versus RXR-MO, Figures 3C and 3D). We also observed a significant increase in the endplate area of NMJs in CPP-MO mice at P15 ($p < 0.001$, Figure 3E), which was maintained at P30, in particular for r6-MO (Figure 3F). SMA mice typically present muscle fiber atrophy and smaller skeletal muscle size, particularly in the intercostal muscles.[24] Our data showed that CPP-MO treatment had beneficial effects on these pathological markers in quadriceps and intercostal muscles (Figures 3G and S2) tested with hematoxylin and eosin staining, showing larger and better organized fibers, with cross-sectional areas quantified in quadriceps significantly higher in CPP-treated mice (Figure 3G; $p < 0.001$). Moreover, treatment with CPP-MOs increased the number of MNs. In spinal cords of mice sacrificed at P10, the number of MNs was significantly higher in CPP-treated mice ($p < 0.001$; Figures 4A and 4B). The increasing trend was also confirmed in CPP-MO-treated mice sacrificed at P30 (Figures 4C and 4D).

Spinal gliosis is also known to be significantly high in SMA mice compared with wild-type mice.[23] We investigated gliosis levels, identified by glial fibrillary acidic protein (GFAP) staining of spinal cord from wild-type mice, scr-MO, and CPP-MO-treated SMA mice (Figure 4E). The quantitative analyses showed higher levels of gliosis in scr-MO mice, while they significantly decreased in CPP-MO mice ($p < 0.001$, Figure 4F). All the experiments demonstrated the superiority of r6-MO compared with RXR-MO in ameliorating phenotype and delivering MO to CNS and peripheral organs.

r6-MO treatment restores liver *Igf1* and *SMN* expression in treated mice

The dysregulation of the *insulin-like growth factor 1 (Igf1)* gene axis and its rescue after systemic ASO administration were reported

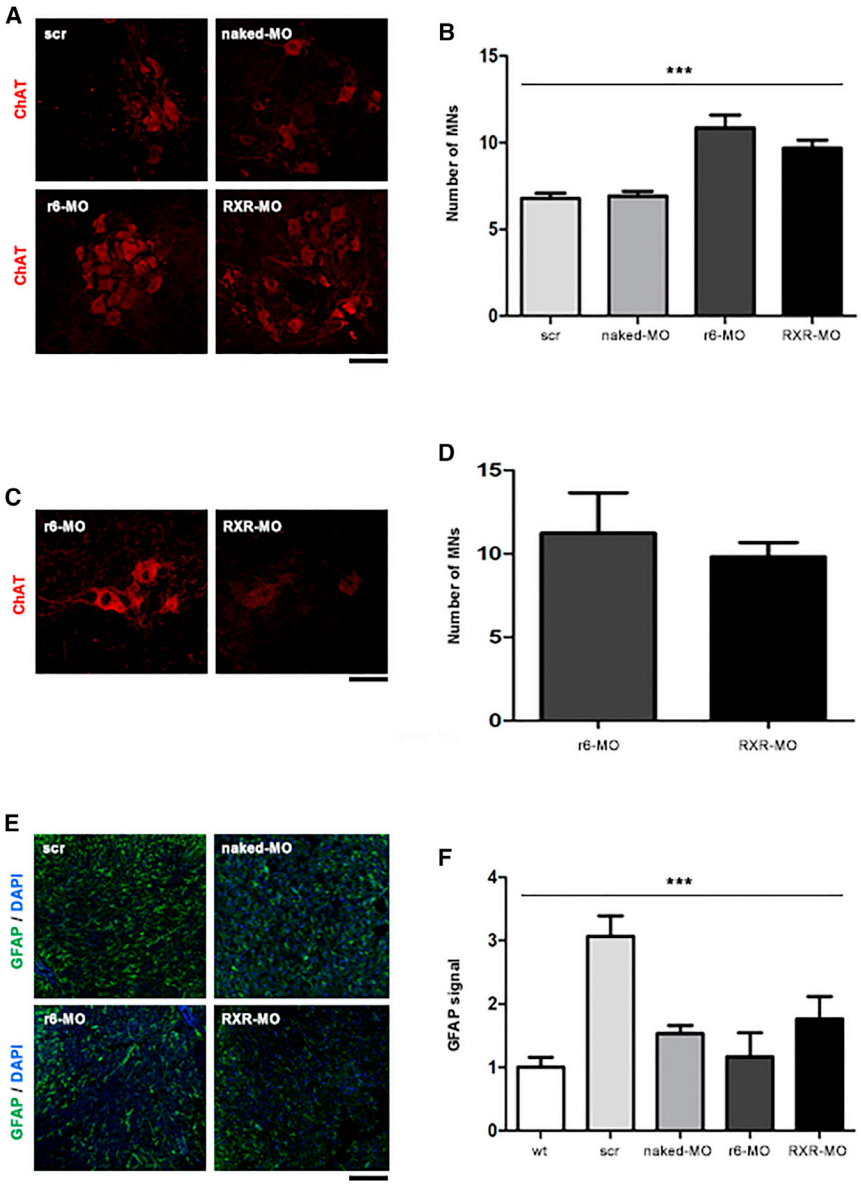

Figure 4. Treatment with CPP-MOs increases MN numbers in the spinal cords of SMA mice

(A) Representative image of MN staining of spinal cords from SMA mice sacrificed at P10. ChAT antibody staining (red) of spinal cord MNs from symptomatic SMA mice treated at P5 with scr, naked MO, r6-MO, or RXR-MO sacrificed at P10. (B) Bar plot of MN numbers in SMA mice spinal cord at P10. Number of MNs was normalized to the scr-MO number as mean ± SEM. Statistical significance was determined using one-way ANOVA (***$p < 0.001$, n = 60 slices, n = 4/group). (C) Representative image of MN staining in spinal cords from SMA mice treated with r6-MO or RXR-MO and sacrificed at P30. (D) Bar plot of MN numbers in spinal cords from SMA mice at P30. (E) Representative image of GFAP staining of spinal cords from wild-type mice and SMA mice treated with scr-MO, naked MO, r6-MO, or RXR-MO and sacrificed at P10. (F) Bar plot of gliosis levels in spinal cords from SMA mice at P10. The number of nuclei surrounded by GFAP was normalized to the scr-MO number and reported as mean ± SEM. Statistical significance was determined using one-way ANOVA (***$p < 0.001$, n = 100 nuclei, n = 4/group). Scale bars, 50 μm (A and C) and 90 μm (E).

previously in an SMA mouse model.[25] We collected livers of treated SMA mice or wild-type mice (n = 4/group) at P7 to see whether the IGF1 pathway was affected in our SMA model and modified by our treatments. Real-time qPCR results showed a significant decrease of both *Igf1* and *insulin growth factor binding protein acid labile subunit* (*Igfals*) expression in scr-MO compared with wild-type mice ($p < 0.001$ and $p < 0.01$, respectively, Figures 5A and 5B). Treatment with r6-MO and RXR-MO tended to increase *Igf1* expression, with significantly higher levels in r6-MO-treated compared with naked MO mice ($p < 0.05$, Figure 5C), while no significant variation was found in *Igfals* expression (Figure 5D).

Notably, real-time qPCR assays performed on spinal cord samples of untreated and treated mice sacrificed at P7 disclosed that the CPP-MOs were able to significantly increase *SMN FL* expression levels ($p < 0.01$, Figure 5E) as well as the *SMN FL*/Δ7 ratios ($p < 0.01$, Figure 5F), indicating that the treatments improved the efficacy of exon 7 inclusion.

DISCUSSION

We conjugated our validated MO 10–34 sequence[15] to CPPs to allow it to reach the CNS by systemic administration even in symptomatic SMA, after the complete closure of the BBB.[25] We used CPPs due to their ability in transporting active biological cargos into the cell.[19] Moreover, the positive charge and arginine content of the most-used CPPs allow them to cross membrane lipid bilayers such as the BBB.[26] CPPs have a demonstrated neuroprotective effect[27] dependent on their positive charge,[28] making them suitable for clinical application with reduced risk of adverse effects.

In this study, we tested four different CPPs conjugated to MO 10–34 for delivery efficiency and toxicity. The two most promising CPPs identified, r6 and RXR, were tested on symptomatic SMA mice using systemic injection. We demonstrated that, even when delivered by IP injection at P5, the r6-MO and RXR-MO conjugates were able to cross the BBB and increase the distribution of MO better than naked MO, resulting in a higher level of SMN, acting increasing exon 7 inclusion. The high internalization efficiency of r6 conjugate likely depends on the lengths of its peptide backbone and stretch of arginine residues,[29] while studies on RXR compound have shown a significant correlation between its splicing correction efficiency and its affinity for heparin

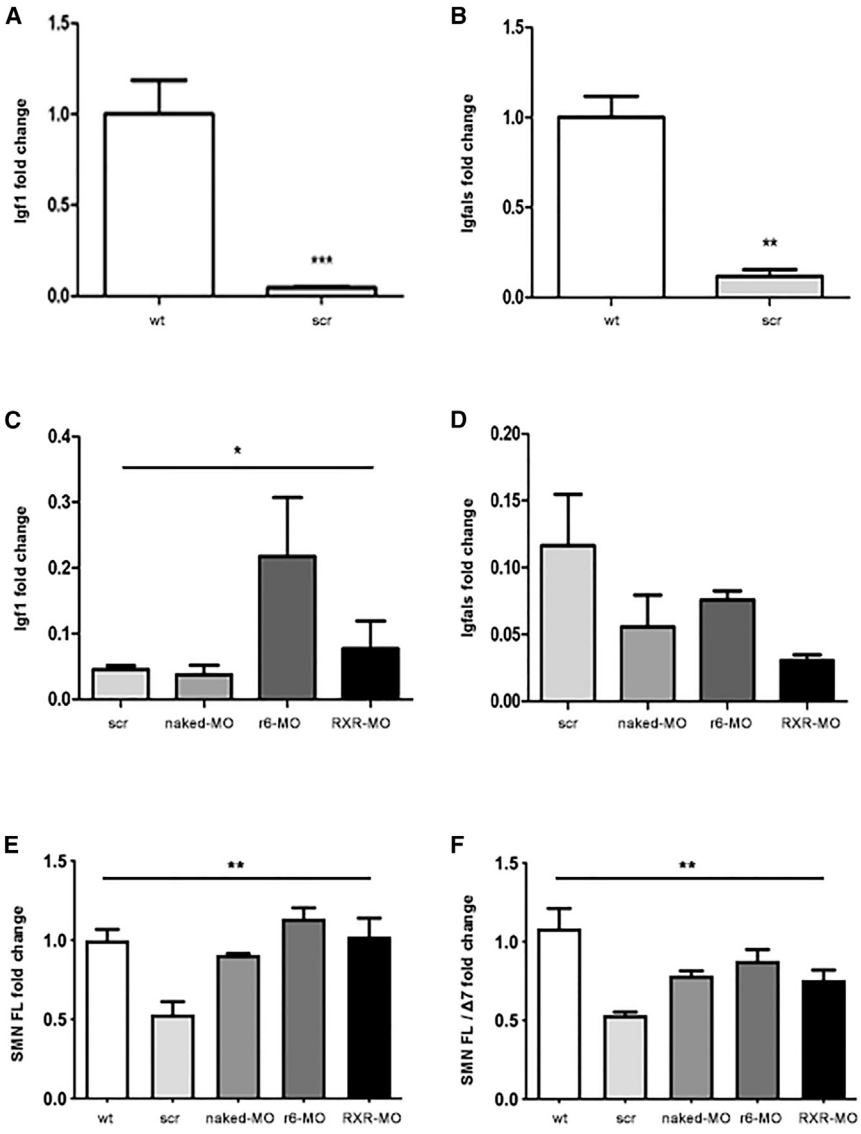

Figure 5. *Igf1*, *Igfals*, *SMN FL*, and *SMN FL/SMN Δ7* expressions are partially restored in CPP-MO-treated mice

(A) Bar plot of liver *Igf1* expression in untreated wild-type mice and scr-MO SMA mice sacrificed at P7 (***$p < 0.001$, Student's t test). (B) Bar plot of liver *Igfals* expression in untreated wild-type mice and scr-MO SMA mice sacrificed at P7 (**$p < 0.01$, Student's t test). (C) Bar plot of liver *Igf1* expression in scr-MO, naked MO, r6-MO, and RXR-MO mice sacrificed at P7 (*$p < 0.05$, ANOVA). (D) Bar plot of liver *Igfals* expression in scr-MO, naked MO, r6-MO, and RXR-MO mice sacrificed at P7. Data were normalized to the average levels of 18S RNA. Values are presented as means ± SEM, at least n = 3/group. (E) Spinal cord *SMN FL* expression in wild-type, scr-MO, naked MO, r6-MO, and RXR-MO mice sacrificed at P7 (**$p < 0.01$, ANOVA). (F) Ratio of *SMN FL/SMN Δ7* expression levels in spinal cord of wild-type, scr-MO, naked MO, r6-MO, and RXR-MO mice sacrificed at P7 (**$p < 0.01$, ANOVA). Data were normalized to the average levels of *B-Actin*. Values are presented as means ± SEM, at least n = 3/group.

and ability to destabilize model synthetic vesicles.[30] A peptide belonging to this particular class has shown promising results in delivering MO in DMD mice by IP injection, with a significantly superior effect on exon skipping and dystrophin restoration compared with the naked MO,[31] while the same peptide ($[RXRRBR]_2XB$), administered by intravenous and intramuscular injection, produced strong dystrophin expression in 100% of fibers in all skeletal muscles examined.[32] We did not observe any toxic effects of our CPP-MOs, confirming what has already been shown for RXR by Jearawiriyapaisarn et al.[33] and for The CPP Pip6 by Hammond et al.[20]

There are very few data about MO compound detection in organs to assess its real biodistribution. We adapted a specific ELISA protocol[34] to detect our MO oligomer, obtaining an innovative method that could be useful in determining the exact effective dose to be administered toward a clinical perspective. We found remarkable amounts of MO in peripheral organs, in particular in liver and heart, suggesting that systemic IP injection promoted dispersion of the conjugate, probably due to the distance of the peritoneum from the brain and spinal cord and its proximity to the liver. We have not excluded the possibility that peripheral SMN restoration played a role in the SMA rescue. Hensel et al. have suggested that peripheral SMN restoration may be needed, complementing SMN restoration in the CNS.[12] In contrast, systemic injection requires a high dose to achieve the right amount of SMN in the CNS: doses lower than 12 nmol/g resulted ineffective. Hammond's group tested lower doses of CPP-MOs, but a comparison with our study is not possible, since the timing and means of administration differ.[20] It would be interesting to explore the efficacy of subcutaneous injection, another systemic delivery, to compare the exact required dose. We used IP delivery for practical reasons in mice, while in humans intravenous injection will be the most likely route of administration. Recently, Sarepta Therapeutics initiated a phase I/IIa clinical trial of a novel MO conjugated to a CPP, PPMO SRP-5051, targeting DMD patients amenable to exon 51 skipping[19] and further supporting the clinical translatability of our proposed CPP-MO injection for SMA.

The analysis of neuropathology revealed that even in mice treated at P5 there was a significant rescue of phenotype. Symptomatic mice treated with CPP-MO conjugates, in comparison with the naked MO, showed improved numbers of innervated NMJs and MNs at

P10, as well as increased NMJ synaptic area, and this improvement was maintained up to P30 and beyond, if we consider the survival and motor ability data. Crucially, this demonstrates that when symptoms are already present, live MNs can be protected from death. NMJs seemed to benefit more from the treatment than MNs. NMJ and MN development are strongly linked, although this connection is not well defined. NMJs are an early pathological target in MN diseases,[35] since SMN protein present in the CNS has a role in their formation and innervation.[36,22] We can speculate that treatment with a CPP-MO, given its increased cell distribution, can more efficiently reverse the deficiency of SMN in spare MNs, protecting and preventing their death even in symptomatic stages. Surviving MNs can then re-innervate NMJs directly or by collateral sprouting. Our treatment can stabilize SMN levels and produce normal-appearing histology in mice up to P30 and beyond, bypassing the developmental period of major SMN requirement. In rodent models of SMA type I, multiple synaptic deficits in the neuromuscular units, including NMJ dysfunction and morphological alterations and central proprioceptive sensory synapses onto MNs have been reported.[37,38] These synaptic defects precede MN loss and the consequent irreversible motor function demise associated with this late event, and may represent the biological basis for functional rescue early in symptomatic disease. It is likely that such cellular dysfunction and cellular loss are also intertwined in humans, although our present understanding is limited by the available therapeutic tools. Furthermore, improvement in NMJ innervation is correlated to decreased muscle atrophy[33] and consequent amelioration of performance in functional tests.

Another aspect we considered is gliosis, which is reported to be associated with areas of MN degeneration in the spinal cord and brain stem in all three types of human SMA, and recent studies suggest that it contributes to MN death.[39,40] Our analyses revealed a strong decrease in GFAP-positive astrocyte numbers in spinal cords of CPP-MO mice compared with scr-MO mice, but not compared with naked MO mice.

Motor skill recovery began around P7, in line with histology showing progress at P10. CPP-MO animals maintained motor functions until death, which occurs suddenly without any evident degeneration. After CPP-MO treatment, survival was significantly extended, with a median of 42 days in r6-MO and 23 days in RXR-MO mice. In CPP-treated groups, 37% of r6-MO-treated animals survived to over 3 months of age, and 25% to over 4 months. To our knowledge, these results have never been achieved before in symptomatic animals with a systemic injection in preclinical testing of therapeutic compounds, whether ASOs, gene therapy, or small molecules. Indeed, the most recent study in symptomatic SMA mice was performed on P2, P4, or P6 by Arnold et al. was not comparable to ours, using ICV injection.[41] Overall, r6-MO proved to be superior to RXR-MO in terms of survival, histopathology, and function. For all treatments, an inter-individual variation was detected in the response to systemic injection, likely resulting from the type of administration and reflecting survival differences observed within each group. Studies using other doses and multiple time points in a larger number of animals are of interest and necessary to optimize this promising therapeutic approach for clinical translation.

The demonstrated phenotypic rescue of symptomatic SMA animals at P5 widened the therapeutic window beyond our expectations, but it is nevertheless still a window, at P7, neither IP nor ICV injection of either CPP-MO had a therapeutic effect. These data are relevant for humans, in which a wider therapeutic window can be expected when the SMN-augmenting compound is distributed well enough to increase the SMN level sufficiently in the majority of cells and the length of the window will still have to be quantified.

Disruption of the IGF1 system has been described in neurodegenerative diseases, including Alzheimer's disease, amyotrophic lateral sclerosis, and SMA.[42] Increasing SMN levels by ASO treatment is reported to re-establish this system.[20,25] Liver *Igf1* and *Igfals* expression levels decreased markedly in SMA compared with unaffected mice. Only *Igf1* expression could be rescued by CPP-MO treatment.

Overall, we demonstrated that the two conjugates, in particular r6-MO, were able to reach the CNS in mice at P5 after IP injection. This avoided invasive intrathecal injection and improved SMN levels and consequently SMA symptoms compared with the naked MO, a novel result in SMA mice. Since symptomatic SMA patients and late-onset mild SMA patients are currently the most difficult to treat, our conjugate should be considered a great improvement from a clinical perspective. Based on the results we obtained, we believe strongly in the feasibility of clinical translation and the utility of the CPP-MO conjugates, even in symptomatic SMA patients.

MATERIALS AND METHODS

MO oligomers

The specific MO sequence targeted to SMN2 pre-mRNA used (GTAAGATTCACTTTCATAATGCTGG) was described previously.[15] The CPPs used in the study are Tat (YGRKKRRQRRRQ), R6 (RRRRRR, L enantiomeric configuration), r6 (RRRRRR, D enantiomeric configuration), and RXR (sequence: $[RXRRBR]_2XB$). Each of the CPP was covalently conjugated to the 5′ end of the MO by our external collaborator, Dr. Hong Moulton, using previously described methods.[30,43] A scramble MO (scr, GTAACATTGACTT TGATATTCCTGG) was used as a control for antisense specificity.

Animal models

All transgenic animals were purchased from The Jackson Laboratory (Bar Harbor, ME, USA). All animal experiments were approved by the University of Milan and Italian Ministry of Health review boards according to the institutional guidelines, in compliance with national (D.I. no. 116, G.U. suppl. 40, February 18, 1992, Circolare no. 8, G.U., 14 Luglio 1994) approved protocol 1007-2016-PR. We used JAX stock no. 005025: FVB.Cg-Grm7Tg(SMN2)89AhmbSmn1tm1Msd Tg(SMN2*delta7)4299Ahmb/J, a mouse model of type I/II SMA, also called SMAΔ7 mouse. Heterozygous animal for Smn1 (Smn+/−; SMN2+/+; SMNΔ7+/+) were bred together to obtain mice that are homozygous knockout for Smn1 allele (Smn−/−) and homozygous for

the other two transgenic alleles (SMN2+/+; SMNΔ7+/+). These mice (Smn−/−; SMN2+/+; SMNΔ7+/+) display SMA phenotype and are named SMA mice. The mice were genotyped with a PCR assay on genomic DNA from tail biopsies, as described previously.[25]

Treatments

Treatments were carried out on cryoanesthetized mice using a 10 μL, 30-gauge Hamilton syringe.

Heterozygous mice

Preliminary treatments were performed on heterozygous SMA mice, to determine the therapeutic efficacy of four different CPPs (n = 6 treated mice per CPP) versus scr-MO and naked MO mice. CPP-conjugated MO was administered at a concentration of 12 nmol/g[15] using ICV or IV protocol[25,44] in SMA mice at P1.

SMA mice

To test the efficacy of our specific treatment on symptomatic SMA mice, 6 (7.5 mg/kg), 9 (11.25 mg/kg), or 12 nmol/g (15 mg/kg) of CPP-MO (n = 21), naked MO (n = 23) and scr-MO (n = 25) were administered in symptomatic SMA mice by IP injection at P5, P7, or P10. To investigate the width of SMA therapeutic window, 12 nmol/g (15 mg/kg) of CPP-MOs, naked MO and scr-MO were administered by ICV injection in SMA mice at P7 (n = 6) as described previously.[21]

WB

For SMN protein detection, treated mice (n = 4 per treatment) were sacrificed 48 h after injection. The following tissues were harvested: brain, spinal cord, kidney, heart, liver. Tissues were frozen in liquid nitrogen and stored at −80°C. Blood was collected and processed for toxicity analyses.

Two different extraction protocols were used depending on tissue type. Brain, kidney, heart, and liver were weighted and extraction buffer (4 M urea, 4% SDS) was added in a concentration of 19 μL/mg. Tissues in suspension were then homogenized. Spinal cord was weighted, and in this case extraction buffer (Tris-HCl 0.5 M, 10%, glycerol 10%, β-mercaptoethanol 0.3%, bromophenol blue 0.3%, SDS 0.3%, protease inhibitor cocktail 0.5%) was added to reach a concentration of 11 μL/mg; spinal cord was sonicated. Dosage of extracted protein was performed using the Lowry method.[45]

Five micrograms of protein was separated by 12% precast SDS-PAGE (Bio-Rad) and electrophoretically transferred to a nitrocellulose membrane (GE Healthcare, Amersham). Membranes were incubated with anti-SMN (1:1,000, BD) and anti-actin (1:1,000, Sigma) antibodies. In particular, secondary anti-mouse IR-DYE 800 CW (1:20,000) were added for 1 h at room temperature (RT), bands were visualized with LI-COR Biosciences technology, Odyssey FC, and densitometric analysis was carried out on Image Studio Software (LI-COR Biosciences).

ELISA

To quantify MO delivered to different organs by the conjugation with either the RXR or r6 peptide, independently from SMN levels, we performed an ELISA method based on a previously described protocol.[34] Naked and r6-MO mice (n = 3/group) were sacrificed 48 h after IP treatment (P7), and the brain (n = 5/group), spinal cord (n = 3/group), liver (n = 3/group), quadriceps muscle (n = 5/group), and heart (n = 3/group) were harvested. After homogenization and trypsin digestion, tissues were eluted and tested in triplicate on a Neutravidin-coated plate at RT overnight and hybridized with a specific probe complementary to our MO sequence (Eurofins). After washing, the plate was incubated with 5 U/well micrococcal nuclease, the optimal enzyme concentration determined for our probe. After incubation with anti-digoxigenin AP-conjugated antibody and subsequently with the AttoPhos substrate, the plate reading was performed using a Varioskan LUX multimode microplate reader (Thermo Fisher Scientific, USA). Four control wells in duplicate were added in each plate to determine the background signal.

Survival and phenotypic tests

Each day, observers monitored all injected animals (wild type n = 6, scr-MO n = 10, naked MO n = 12, r6-MO, or RXR-MO n = 8/group), as well as breeding pairs, for morbidity, mortality, and weight. All treated animals underwent phenotypic tests and weight measures twice a week up to P14, then weight was measured once a week.

Hindlimb suspension test

Hindlimb suspension test evaluates the positioning of the legs and tail. Mice were suspended by their hind limbs from the lip of a standard 50-mL plastic centrifuge tube. The posture was scored from 0 to 4 as described previously.[46]

Righting reflex

Righting reflex assay was performed turning each pup onto its back and evaluating its ability to stably place all four paws on the ground.[46]

Rotarod

The rotarod test (RotaRod 7650; Ugo Basile) was performed from P45 once a month, using a 4-phase profile as described previously.[15]

Histological analyses

For immunohistochemistry analyses, untreated mice at P5 and treated/scr mice at P10 or P30 were sacrificed (at least n = 3/group). Intercostal muscles were directly frozen on dry ice, while spinal cord samples were fixed in paraformaldehyde (PFA) 4% for 24 h. The next day PFA was removed, tissues were washed in PBS 1× and put in 30% sucrose for 24 h. Then, spinal cord was extracted from the column, lumbar section was cut and frozen in dry ice and at −80°C. At least 24 h after freezing, both tissues were cryosectioned on SuperFrost microscope slides. The section thickness was 20 μm.

NMJ detection

To detect innervated NMJs in intercostal muscles, we added to the slides 10% normal goat serum (NGS) in PBS 1× and 0.3% Triton X-100 for 1 h at RT. Primary antibodies were added overnight at 4°C: neurofilament 1 (1:250; Milllipore) and α-bungarotoxin 555 (1:200; Life Technologies). With unconjugated primary antibody,

we used mouse and rabbit secondary antibodies conjugated with Alexa 488 (1:1,000, Life Technologies) for 1 h at RT. After washing three times in PBS 1× the coverslips were mounted with the use of FluorSave Reagent (Calbiochem). Images of the stained intercostal muscles were acquired with a confocal microscope LEICA SP8. We counted the total number of NMJs and the percentage that was innervated by the axons, when the two signals merged. As already described, we considered at least 100 NMJs from each muscle.[15]

Endplate area

We used intercostal muscles stained for α-bungarotoxin 555. Images acquired by confocal microscopy were analyzed with ImageJ software: endplate areas marked by α-bungarotoxin were encircled/trimmed with a specific tool and measured in at least 100 NMJs, as described previously.[47]

MN detection

To evaluate the number of MNs in spinal cord (n = 4/group) in immunofluorescence, slices were blocked in PBS 1× with 10% NGS and 0.3% Triton X-100 for 1 h at RT. We stained sections taken from at least 100 μm apart to avoid double counting of the same cell. Primary antibody ChAT (goat 1:250, Millipore) was added overnight at 4°C, then the slides were incubated for 1.5 h at RT with the specific secondary biotinylated antibody (1:400, Vector Laboratories), then they were incubated for 1 h at RT with Streptavidin Cy3 (1:400, Sigma Aldrich). Counts were made in the anterior ventral horns of the spinal cord and serial sections (n = 30 slices for each zone L1-L2, L3-L5, which resulted in four to six slides per mouse) were analyzed at 20× magnification.

Gliosis

To assess the presence of gliosis in the spinal cord of mice (n = 4/group), we blocked slices in PBS 1× with 10% NGS and 0.3% Triton X-100 for 1 h at RT. GFAP primary antibody (1:500, Abcam) was added overnight at 4°C, then the slides were incubated with Alexa 488 secondary antibody (1:1,000, Life Technologies) for 1.5 h at RT. Once the cover slides were mounted, to perform a semi-quantitative analysis, we acquired from four to six images of spinal cord half slices for each treatment at 20× with a confocal microscope (LEICA SP8), to count at least n = 100 nuclei, and divided the number of nuclei surrounded by more than 50% of their perimeter by GFAP by the total number of cells.[48]

Staining of muscle fibers

We performed a hematoxylin and eosin staining on intercostal muscle slices of CPP MO-treated, naked MO-treated, and scramble mice: slides were incubated for 50 s in hematoxylin reagent, and washed in water. Then slides were stained in eosin reagent for 20 s, rinsed, incubated in EtOH for 5 min, and washed twice in EtOH. Finally, slides were rinsed three times in xylene and mounted with cover slides.

Cross-sectional area

To measure the cross-sectional area of muscle fibers, pictures of hematoxylin and eosin staining were acquired by optical microscopy and perimeters of fibers were encircled/trimmed using ImageJ. Areas were measured as described previously[49] for at least 100 fibers.

RNA isolation and real-time qPCR

Wild-type and SMA mice (scr-MO, naked MO, r6-MO, RXR-MO) were sacrificed 48 h after IP treatment at P5. Total RNA was extracted from murine livers (at least n = 3/group) using ReliaPrep RNA Tissue Miniprep System (Promega). cDNA for real-time PCR experiments was synthesized from 1.5 μg of total RNA, using the Ready-To-Go kit (GE Healthcare). The expression levels of *Igf1* (Mm00439559_m1, Thermo Fisher Scientific), *Igfals* (Mm01962637_s1, Thermo Fisher Scientific), *SMN FL*, and *SMN Δ7* (probes and primers available upon request) were assessed by quantitative analysis on a 7500 Real-Time PCR System (Applied Biosystems). Data were normalized to the average levels of *18S* (Hs99999901_s1, Thermo Fisher Scientific) or *B-Actin* (Mm00607939_s1, Thermo Fisher Scientific).

Toxicity evaluation of the CPP-MO conjugates

To assess the toxicity of the CPP-MO treatments we collect the blood from wild type mice (n = 11) with SMA treated with r6-PMO, RXR-PMO, or scr-MO (n = 3/group) during the dissection procedure. The blood was left for 30 min at RT and then centrifuged for 10 min at 3,500 rcf. The resulting supernatant, the serum, was transferred in a new tube and stored at −20°C.

The evaluation was performed by Charles River Laboratories on a standard set of toxicity biomarkers: glucose, creatinine, urea, total cholesterol, total protein, total bilirubin, alkaline phosphatase, alanine transaminase, creatine kinase, and lactate dehydrogenase.

Statistical analyses

All statistical analyses were performed using the Prism software. Data were expressed as mean ± standard error of the mean (SEM). All data were analyzed using one-way ANOVA for multi-comparison analyses followed by Tukey post-hoc tests and Student's t test to compare each CPP-MO treatment with naked MO. NMJ innervation and righting test were analyzed using a contingency test following by Fisher's exact test. Kaplan-Meier survival analysis and log rank test were used for survival comparisons. Values were considered significant when $p < 0.05$.

SUPPLEMENTAL INFORMATION

Supplemental information can be found online at https://doi.org/10.1016/j.ymthe.2021.11.012.

ACKNOWLEDGMENTS

The authors thank the Associazione Amici del Centro Dino Ferrari for its support. This study was supported by Telethon Foundation to M.N., GGP14025, Research and Innovation Staff Exchange (RISE) CROSS-NEUROD grant no. 778003 to S.C. and Italian Ministry of Health Foundation IRCCS Ca' Granda Ospedale Maggiore Policlinico Ricerca Corrente 2020 to G.P.C. and N.B.

AUTHOR CONTRIBUTIONS

M.B. and E.P. conceived and performed the experiments and the data analysis for Figures 2, 3, and 4 and associated supplemental data, and participated in manuscript writing. M.R. conducted the experiments and provided data for Figure 5 and participated in data analysis, figures design, and manuscript writing. D.S. conducted the ELISA assay and provided data for Figure 1F. M.G. conducted WB analyses and provided data for Figure 1. H.M.M. developed Morpholino technology oligomers and performed the linkage to the CPPs. M.N. and S.C. conceived the study, designed the research, and reviewed the draft. G.P.C. and N.B. provided resources. All co-authors provided discussion and data interpretation and contributed to the final version of the manuscript.

DECLARATION OF INTERESTS

The authors declare no competing interests.

REFERENCES

1. D'Amico, A., Mercuri, E., Tiziano, F.D., and Bertini, E. (2011). Spinal muscular atrophy. Orphanet J. Rare Dis. *6*, 71. https://doi.org/10.1186/1750-1172-6-71.
2. Lefebvre, S., Bürglen, L., Reboullet, S., Clermont, O., Burlet, P., Viollet, L., Benichou, B., Cruaud, C., Millasseau, P., Zeviani, M., Paslier, D.L., Fr6zal, J., Cohen, D., Weissenbach, J., Munnich, A., and Judith Melki, J. (1995). Identification and characterization of a spinal muscular atrophy-determining gene. Cell *80*, 155–165. https://doi.org/10.1016/0092-8674(95)90460-3.
3. Monani, U.R., Lorson, C.L., Parsons, D.W., Prior, T.W., Androphy, E.J., Burghes, A.H., and McPherson, J.D. (1999). A single nucleotide difference that alters splicing patterns distinguishes the SMA gene SMN1 from the copy gene SMN2. Hum. Mol. Genet. *8*, 1177–1183. https://doi.org/10.1093/hmg/8.7.1177.
4. Maretina, M.A., Zheleznyakova, G.Y., Lanko, K.M., Egorova, A.A., Baranov, V.S., and Kiselev, A.V. (2018). Molecular factors involved in spinal muscular atrophy pathways as possible disease-modifying candidates. Curr. Genomics *19*, 339–355. https://doi.org/10.2174/1389202919666180101154916.
5. Claborn, M.K., Stevens, D.L., Walker, C.K., and Gildon, B.L. (2019). Nusinersen: a treatment for spinal muscular atrophy. Ann. Pharmacother. *53*, 61–69. https://doi.org/10.1177/1060028018789956.
6. Schorling, D.C., Pechmann, A., and Kirschner, J. (2020). Advances in treatment of spinal muscular atrophy——new phenotypes, new challenges, new implications for care. J. Neuromuscul. Dis. *7*, 1–13. https://doi.org/10.3233/JND-190424.
7. Wurster, C.D., Winter, B., Wollinsky, K., Ludolph, A.C., Uzelac, Z., Witzel, S., Schocke, M., Schneider, R., and Kocak, T. (2019). Intrathecal administration of nusinersen in adolescent and adult SMA type 2 and 3 patients. J. Neurol. *266*, 183–194. https://doi.org/10.1007/s00415-018-9124-0.
8. Mercuri, E., Darras, B.T., Chiriboga, C.A., Day, J.W., Campbell, C., Connolly, A.M., Iannaccone, S.T., Kirschner, J., Kuntz, N.L., Saito, K., Shieh, P.B., Tulinius, M., Mazzone, E.S., Montes, J., Bishop, K.M., Yang, Q., Foster, R., Gheuens, S., Bennett, C.F., Farwell, W., Schneider, E., De Vivo, D.C., and Finkel, R.S.; CHERISH Study Group (2018). Nusinersen versus sham control in later-onset spinal muscular atrophy. N. Engl. J. Med. *378*, 625–635. https://doi.org/10.1056/NEJMoa1710504.
9. Wadman, R.I., van der Pol, W.L., Bosboom, W.M., Asselman, F.L., van den Berg, L.H., Iannaccone, S.T., and Vrancken, A.F. (2020). Drug treatment for spinal muscular atrophy types II and III. Cochrane Database Syst. Rev. *1*, CD006282. https://doi.org/10.1002/14651858.CD006282.
10. Parente, V., and Corti, S. (2018). Advances in spinal muscular atrophy therapeutics. Ther. Adv. Neurol. Disord. *11*. 1756285618754501. https://doi.org/10.1177/1756285618754501.
11. Dangouloff, T., and Servais, L. (2019). Clinical evidence supporting early treatment of patients with spinal muscular atrophy: current perspectives. Ther. Clin. Risk Manag. *15*, 1153–1161. https://doi.org/10.2147/TCRM.S172291.
12. Hensel, N., Kubinski, S., and Claus, P. (2020). The need for SMN-independent treatments of spinal muscular atrophy (SMA) to complement SMN-enhancing drugs. Front. Neurol. *11*, 45. https://doi.org/10.3389/fneur.2020.00045.
13. Ramos, D.M., d'Ydewalle, C., Gabbeta, V., Dakka, A., Klein, S.K., Norris, D.A., Matson, J., Taylor, S.J., Zaworski, P.G., Prior, T.W., Snyder, P.J., Valdivia, D., Hatem, C.L., Waters, I., Gupte, N., Swoboda, K.J., Rigo, F., Bennett, C.F., Naryshkin, N., Paushkin, S., Crawford, T.O., and Sumner, C.J. (2019). Age-dependent SMN expression in disease-relevant tissue and implications for SMA treatment. J. Clin. Invest. *129*, 4817–4831. https://doi.org/10.1172/JCI124120.
14. Porensky, P.N., and Burghes, A.H. (2013). Antisense oligonucleotides for the treatment of spinal muscular atrophy. Hum. Gene Ther. *24*, 489–498. https://doi.org/10.1089/hum.2012.225.
15. Nizzardo, M., Simone, C., Salani, S., Ruepp, M.D., Rizzo, F., Ruggieri, M., Zanetta, C., Brajkovic, S., Moulton, H.M., Müehlemann, O., Bresolin, N., Comi, G.P., and Corti, S. (2014). Effect of combined systemic and local morpholino treatment on the spinal muscular atrophy Δ7 mouse model phenotype. Clin. Ther. *36*, 340–356.e5. https://doi.org/10.1016/j.clinthera.2014.02.004.
16. Foged, C., and Nielsen, H.M. (2008). Cell-penetrating peptides for drug delivery across membrane barriers. Expert Opin. Drug Deliv. *5*, 105–117. https://doi.org/10.1517/17425247.5.1.105. PMID: 18095931.
17. Lebleu, B., Moulton, H.M., Abes, R., Ivanova, G.D., Abes, S., Stein, D.A., Iversen, P.L., Arzumanov, A.A., and Gait, M.J. (2008). Cell penetrating peptide conjugates of steric block oligonucleotides. Adv. Drug Deliv. Rev. *60*, 517–529. https://doi.org/10.1016/j.addr.2007.09.002.
18. Moulton, H.M., and Moulton, J.D. (2010). Morpholinos and their peptide conjugates: therapeutic promise and challenge for Duchenne muscular dystrophy. Biochim. Biophys. Acta *1798*, 2296–2303. https://doi.org/10.1016/j.bbamem.2010.02.012.
19. Tsoumpra, M.K., Fukumoto, S., Matsumoto, T., Takeda, S., Wood, M.,A., and Aoki, Y. (2019). Peptide-conjugate antisense based splice-correction for Duchenne muscular dystrophy and other neuromuscular diseases. EBioMedicine *45*, 630–645. https://doi.org/10.1016/j.ebiom.2019.06.036.
20. Hammond, S.M., Hazell, G., Shabanpoor, F., Saleh, A.F., Bowerman, M., Sleigh, J.N., Meijboom, K.E., Zhou, H., Muntoni, F., Talbot, K., Gait, M.J., and Wood, M.J. (2016). Systemic peptide-mediated oligonucleotide therapy improves long-term survival in spinal muscular atrophy. Proc. Natl. Acad. Sci. U S A. *113*, 10962–10967. https://doi.org/10.1073/pnas.1605731113.
21. Shabanpoor, F., Hammond, S.M., Abendroth, F., Hazell, G., Wood, M., and Gait, M.J. (2017). Identification of a peptide for systemic brain delivery of a morpholino oligonucleotide in mouse models of spinal muscular atrophy. Nucleic Acid Ther. *27*, 130–143. https://doi.org/10.1089/nat.2016.0652.
22. Kariya, S., Park, G.H., Maeno-Hikichi, Y., Leykekhman, O., Lutz, C., Arkovitz, M.S., Landmesser, L.T., and Monani, U.R. (2008). Reduced SMN protein impairs maturation of the neuromuscular junctions in mouse models of spinal muscular atrophy. Hum. Mol. Genet. *17*, 2552–2569. https://doi.org/10.1093/hmg/ddn156.
23. d'Errico, P., Boido, M., Piras, A., Valsecchi, V., De Amicis, E., Locatelli, D., Capra, S., Vagni, F., Vercelli, A., and Battaglia, G. (2013). Selective vulnerability of spinal and cortical motor neuron subpopulations in delta7 SMA mice. PloS one *8*, e82654. https://doi.org/10.1371/journal.pone.0082654.
24. Le, T.T., Pham, L.T., Butchbach, M.E., Zhang, H.L., Monani, U.R., Coovert, D.D., Gavrilina, T.O., Xing, L., Bassell, G.J., and Burghes, A.H. (2005). SMNDelta7, the major product of the centromeric survival motor neuron (SMN2) gene, extends survival in mice with spinal muscular atrophy and associates with full-length SMN. Hum. Mol. Genet. *14*, 845–857. https://doi.org/10.1093/hmg/ddi078.
25. Hua, Y., Sahashi, K., Rigo, F., Hung, G., Horev, G., Bennett, C.F., and Krainer, A.R. (2011). Peripheral SMN restoration is essential for long-term rescue of a severe spinal muscular atrophy mouse model. Nature *478*, 123–126. https://doi.org/10.1038/nature10485.
26. Zou, L.L., Ma, J.L., Wang, T., Yang, T.B., and Liu, C.B. (2013). Cell-penetrating peptide-mediated therapeutic molecule delivery into the central nervous system. Curr. Neuropharmacol. *11*, 197–208. https://doi.org/10.2174/1570159X11311020006.
27. Meloni, B.P., Mastaglia, F.L., and Knuckey, N.W. (2020). Cationic arginine-rich peptides (CARPs): a novel class of neuroprotective agents with a multimodal mechanism of action. Front. Neurol. *11*, 108. https://doi.org/10.3389/fneur.2020.00108.

28. McQueen, J., Ryan, T.J., McKay, S., Marwick, K., Baxter, P., Carpanini, S.M., Wishart, T.M., Gillingwater, T.H., Manson, J.C., Wyllie, D.J.A., Grant, S.G.N., McColl, B.W., Komiyama, N.H., and Hardingham, G.E. (2017). Pro-death NMDA receptor signaling is promoted by the GluN2B C-terminus independently of Dapk1. eLife *6*, e17161. https://doi.org/10.7554/eLife.17161.

29. Kerkis, A., Hayashi, M.A., Yamane, T., and Kerkis, I. (2006). Properties of cell penetrating peptides (CPPs). IUBMB life *58*, 7–13. https://doi.org/10.1080/15216540500494508.

30. Abes, S., Moulton, H.M., Clair, P., Prevot, P., Youngblood, D.S., Wu, R.P., Iversen, P.L., and Lebleu, B. (2006). Vectorization of morpholino oligomers by the (R-Ahx-R)4 peptide allows efficient splicing correction in the absence of endosomolytic agents. J. Control Release: Official J. Control Release Soc. *116*, 304–313. https://doi.org/10.1016/j.jconrel.2006.09.011.

31. Fletcher, S., Honeyman, K., Fall, A.M., Harding, P.L., Johnsen, R.D., Steinhaus, J.P., Moulton, H.M., Iversen, P.L., and Wilton, S.D. (2007). Morpholino oligomer-mediated exon skipping averts the onset of dystrophic pathology in the mdx mouse. Mol. Ther. J. Am. Soc. Gene Ther. *15*, 1587–1592. https://doi.org/10.1038/sj.mt.6300245.

32. Wu, B., Moulton, H.M., Iversen, P.L., Jiang, J., Li, J., Li, J., Spurney, C.F., Sali, A., Guerron, A.D., Nagaraju, K., Doran, T., Lu, P., Xiao, X., and Lu, Q.L. (2008). Effective rescue of dystrophin improves cardiac function in dystrophin-deficient mice by a modified morpholino oligomer. Proc. Natl. Acad. Sci. U S A. *105*, 14814–14819. https://doi.org/10.1073/pnas.0805676105.

33. Jearawiriyapaisarn, N., Moulton, H.M., Buckley, B., Roberts, J., Sazani, P., Fucharoen, S., Iversen, P.L., and Kole, R. (2008). Sustained dystrophin expression induced by peptide-conjugated morpholino oligomers in the muscles of mdx mice. Mol. Ther. J. Am. Soc. Gene Ther. *16*, 1624–1629. https://doi.org/10.1038/mt.2008.120.

34. Burki, U., Keane, J., Blain, A., O'Donovan, L., Gait, M.J., Laval, S.H., and Straub, V. (2015). Development and application of an ultrasensitive hybridization-based ELISA method for the determination of peptide-conjugated phosphorodiamidate morpholino oligonucleotides. Nucleic Acid Ther. *25*, 275–284. https://doi.org/10.1089/nat.2014.0528.

35. Boido, M., and Vercelli, A. (2016). Neuromuscular junctions as key contributors and therapeutic targets in spinal muscular atrophy. Front. Neuroanat. *10*, 6. https://doi.org/10.3389/fnana.2016.00006.

36. Zhang, Z., Pinto, A.M., Wan, L., Wang, W., Berg, M.G., Oliva, I., Singh, L.N., Dengler, C., Wei, Z., and Dreyfuss, G. (2013). Dysregulation of synaptogenesis genes antecedes motor neuron pathology in spinal muscular atrophy. Proc. Natl. Acad. Sci. U S A. *110*, 19348–19353. https://doi.org/10.1073/pnas.1319280110.

37. Shorrock, H.K., Gillingwater, T.H., and Groen, E. (2019). Molecular mechanisms underlying sensory-motor circuit dysfunction in SMA. Front. Mol. Neurosci. *12*, 59. https://doi.org/10.3389/fnmol.2019.00059.

38. Van Alstyne, M., and Pellizzoni, L. (2016). Advances in modeling and treating spinal muscular atrophy. Curr. Opin. Neurol. *29*, 549–556. https://doi.org/10.1097/WCO.0000000000000368.

39. Wang, D.D., and Bordey, A. (2008). The astrocyte odyssey. Prog. Neurobiol. *86*, 342–367. https://doi.org/10.1016/j.pneurobio.2008.09.015.

40. Abati, E., Citterio, G., Bresolin, N., Comi, G.P., and Corti, S. (2020). Glial cells involvement in spinal muscular atrophy: could SMA be a neuroinflammatory disease? Neurobiol. Dis. *140*, 104870. https://doi.org/10.1016/j.nbd.2020.104870.

41. Arnold, W., McGovern, V.L., Sanchez, B., Li, J., Corlett, K.M., Kolb, S.J., Rutkove, S.B., and Burghes, A.H. (2016). The neuromuscular impact of symptomatic SMN restoration in a mouse model of spinal muscular atrophy. Neurobiol. Dis. *87*, 116–123. https://doi.org/10.1016/j.nbd.2015.12.014.

42. Trejo, J.L., Carro, E., Garcia-Galloway, E., and Torres-Aleman, I. (2004). Role of insulin-like growth factor I signaling in neurodegenerative diseases. J. Mol. Med. (Berlin, Germany) *82*, 156–162. https://doi.org/10.1007/s00109-003-0499-7.

43. Moulton, H.M., Hase, M.C., Smith, K.M., and Iversen, P.L. (2003). HIV Tat peptide enhances cellular delivery of antisense morpholino oligomers. Antisense Nucleic Acid Drug Dev. *13*, 31–43. https://doi.org/10.1089/108729003764097322.

44. Gombash, S.E., Cowley, C.J., Fitzgerald, J.A., Hall, J.C., Mueller, C., Christofi, F.L., and Foust, K.D. (2014). Intravenous AAV9 efficiently transduces myenteric neurons in neonate and juvenile mice. Front. Mol. Neurosci. *7*, 81. https://doi.org/10.3389/fnmol.2014.00081.

45. Waterborg, J.H., and Matthews, H.R. (1984). The Lowry method for protein quantitation. Methods Mol. Biol. (Clifton, N.J.) *1*, 1–3. https://doi.org/10.1385/0-89603-062-8:1.

46. Butchbach, M.E., Edwards, J.D., and Burghes, A.H. (2007). Abnormal motor phenotype in the SMNDelta7 mouse model of spinal muscular atrophy. Neurobiol. Dis. *27*, 207–219. https://doi.org/10.1016/j.nbd.2007.04.009.

47. Valsecchi, V., Boido, M., De Amicis, E., Piras, A., and Vercelli, A. (2015). Expression of muscle-specific MiRNA 206 in the progression of disease in a murine SMA model. PLoS One *10*, e0128560. https://doi.org/10.1371/journal.pone.0128560.

48. Jalenques, I., Albuisson, E., Despres, G., and Romand, R. (1995). Distribution of glial fibrillary acidic protein (GFAP) in the cochlear nucleus of adult and aged rats. Brain Res. *686*, 223–232. https://doi.org/10.1016/0006-8993(95)00463-Z.

49. DeChick, A., Hetz, R., Lee, J., and Speelman, D.L. (2020). Increased skeletal muscle fiber cross-sectional area, muscle phenotype shift, and altered insulin signaling in rat hindlimb muscles in a prenatally androgenized rat model for polycystic ovary syndrome. Int. J. Mol. Sci. *21*, 7918. https://doi.org/10.3390/ijms21217918.